CHEMISTRY OF MATERIALS

pubs.acs.org/cm

Article

Phase-Pure Zirconium Metal−Organic Polyhedra Enabled by a Ligand Substitution Strategy

Meghan G. Sullivan, Heshali K. Welgama, Matthew R. Crawley, Alan E. Friedman, and Timothy R. Cook*

Cite This: *Chem. Mater.* 2024, 36, 567−574

Read Online

ACCESS | Metrics & More | Article Recommendations | Supporting Information

ABSTRACT: Zirconium-based metal−organic polyhedra (ZrMOPs) are attractive due to their high stabilities, low-cost building blocks, and solubilities relative to their metal−organic framework analogues (e.g., UiO-66); although these sorts of self-assembled cages often form single thermodynamic products, ZrMOP architectures are typically plagued by the formation of both V_4L_6 "tetrahedra" and V_2L_3 "lanterns" (V = vertex, L = ligand) as coproducts of their syntheses. In this work, we demonstrate a ligand-exchange strategy to isolate previously inaccessible phase-pure ZrMOPs using two different dicarboxylate donors. We also describe characterization methods that can be used to discriminate between the two architectures to confirm our approach provides synthetic selectivity. The phase-pure materials were found to have drastically different Brunauer−Emmett−Teller (BET) areas, with lanterns exhibiting significantly smaller surface areas (4−20 m^2/g) than the tetrahedral architectures (393−605 m^2/g), irrespective of counterions or bridging dicarboxylates. By obviating mixed-phase products of synthesis, our generalizable ligand-exchange pathway to phase-pure ZrMOPs enables systematic fundamental studies and will advance the functional use of these materials.

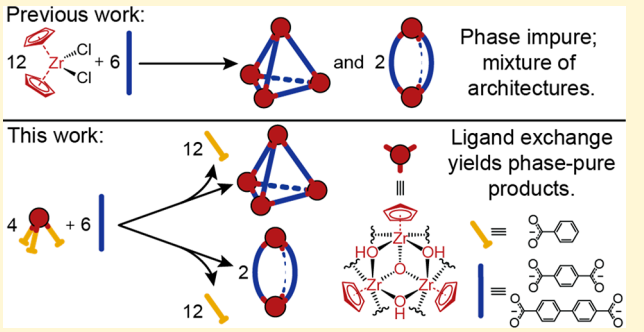

INTRODUCTION

Self-assembly is commonly used to make porous inorganic materials.[1] In many cases, the final architecture can be predicted from the structure of the molecular starting materials, or the "building blocks".[2,3] Because this process is modular, chemists have explored porous materials using self-assembly as both extended coordination polymers (e.g., metal−organic frameworks, MOFs) and discrete molecules (e.g., metal−organic polyhedra, MOPs). Generally, this modular assembly makes MOFs and MOPs tunable by simply changing to different donor or acceptor moieties, which imparts new functionality and material properties, such as changes to surface area and porosity. These features underpin applications in gas separation,[4−7] catalysis,[8−10] water purification,[11−14] biomedicine,[15−18] and energy storage.[19,20]

Although metal−organic materials are tunable and may exhibit high surface areas, many suffer from hydrolytic and/or thermal instability.[21−23] Zirconium-based MOPs are notable among these materials for their high stabilities, high-yielding syntheses, and low-cost building blocks. In addition, research into MOPs is often motivated by their higher solubilities relative to MOFs because they are molecular in nature.[24,25] ZrMOPs have shown stability in both basic and acidic media and at temperatures up to 300 °C.[26,27] The synthesis of ZrMOPs can be done under atmospheric conditions and requires only zirconocene dichloride with a simple dicarboxylate ligand in addition to the solvent, making the process both easy and inexpensive.[28] For these reasons, ZrMOPs have been studied to address a wide range of applications including sensing,[29−31] catalysis,[32−36] biomedicine,[37−39] guest capture,[29,40] and gas separation/storage.[41−45]

Despite their promise, traditional syntheses of ZrMOPs often yield a mixture of tetrahedral and so-called cigar or lantern type architectures. In 2020, the Bloch group explored how ligand geometry influences the presence of tetrahedron/lantern or a mixture thereof.[46] For approximately half of the ligands used, mixed-phase products were isolated. In some cases, the chemistry of these materials is developed with the mixtures or focuses on a smaller library of ligands under traditional synthetic conditions (Figure 1).[47,48] Accessing phase-pure ZrMOPs is crucial to properly attribute the properties of tetrahedra versus lantern architectures. This is particularly important for applications where the surface area, pore size, and stability are factors in materials design. There is

Received: October 27, 2023
Revised: December 5, 2023
Accepted: December 11, 2023
Published: December 29, 2023

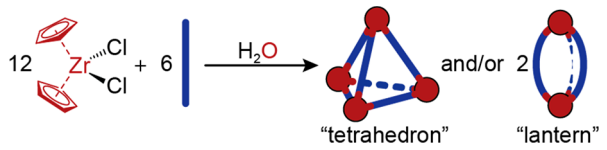

Figure 1. Common synthetic route to the ZrMOP mixtures. Blue lines represent a 180° dicarboxylate ligand, and red circles represent a $Zr_3Cp_3O(OH)_3$ node cluster.

an outstanding need for methods that deliver phase-control over the ZrMOP synthesis.

Ligand exchange is a synthetic method commonly employed in the MOF community to correct defects within frameworks, to add surface functionality to nanoparticles, and to make cross-linked composite materials.[49−52] UiO-66, a Zr-based MOF,[53] is shown to undergo postsynthetic ligand exchange at room temperature,[54−56] yet ligand exchange has not been explored for ZrMOPs as a synthetic route or a postsynthetic modification method.

The traditional synthesis of ZrMOPs has two steps occurring in situ. First, zirconocene dichloride undergoes hydrolysis to form a Zr oxo cluster. Second, dicarboxylates bridge these clusters to deliver polyhedral products. We investigated how ligand exchange may be used to synthesize ZrMOPs, wherein the first hydrolysis step is decoupled from the self-assembly step. A ZrCluster was synthesized with benzoate capping ligands.[57] This ZrCluster was then mixed with stoichiometric equivalents of dicarboxylic acids. Ligand exchange of the benzoic acid caps for the dicarboxylates resulted in the formation of phase-pure ZrMOPs (Scheme 1). This ligand-exchange process was explored for both chloride and triflate counterions and with 1,4-benzenedicarboxylate and biphenyl-4,4′-dicarboxylate ligands.

Separating the cluster formation from the self-assembly enabled optimization of self-assembly conditions and isolation of phase-pure materials. Herein, we report the ligand-exchange conditions and characterization of the phase-pure materials using $^1H/^{19}F$/DOSY NMR and mass spectrometry. Brunauer−Emmett−Teller (BET) areas were measured to compare the tetrahedral ZrMOPs to their lantern analogues. We show that tetrahedra have significantly larger surface areas than lanterns, and this general trend was shown to be independent of the counterion (Cl^-/OTf^-) and bridging ligand.

EXPERIMENTAL SECTION

Materials. Zirconocene dichloride (Cp_2ZrCl_2) and silver trifluoromethanesulfonate (AgOTf) were purchased from Strem Chemicals. Benzoic acid, acetone, and dichloromethane were purchased from Fisher Scientific. 1,4-Benzenedicarboxylic acid (terephthalic acid/1,4-bdc) was purchased from TCI. Biphenyl-4,4′-dicarboxylic acid was purchased from Matrix Scientific. *N*,*N*-Dimethylformamide (DMF) and methanol were purchased from Macron Fine Chemicals. Hydrochloric acid and diethyl ether were purchased from Sigma-Aldrich. All chemicals were used as received without further drying or purification, unless otherwise noted.

Methods. ^1H and $^{19}F\{^1H\}$ nuclear magnetic resonance (NMR) spectra were acquired in 32 scans using a Bruker AVANCE NEO 500 spectrometer in DMSO-d_6. Chemical shifts (δ) are reported in parts per million (ppm) referenced using the residual proton solvent peaks. Multiplicities are indicated as singlets (s), doublets (d), triplets (t), or multiplets (m). Fourier transform infrared (FTIR) spectra were acquired with a PerkinElmer 1760 FTIR spectrometer with horizontal attenuated total reflectance (ATR) and baseline correction on neat powders. All mass spectrometry samples were prepared in methanol. For ESI high-resolution mass spectrometry (HRMS), samples were directly infused to a Thermo Scientific LTQ-OrbitrapXL using an onboard syringe pump, and data were accumulated using the FTMS (orbitrap) at a resolution of 100000. Full spectra can be found in the Supporting Information.

ZrClusters. *[ZrCluster]Cl.* Synthesis was adapted from a literature reported procedure.[57] Benzoic acid (1.67 g, 13.7 mmol, 1 equiv) was mixed with H_2O (68 mL) in a 100 mL round-bottom flask (RBF). Sodium hydroxide (602 mg, 15.1 mmol, 1.1 equiv) was added, and the mixture was stirred until all solid had dissolved. The pH was adjusted by adding concentrated HCl dropwise to the solution, where a final pH of 6−7 was indicated by a white precipitate that persisted. In a separate 500 mL RBF, zirconocene dichloride (4.00 g, 13.7 mmol, 1 equiv) was dissolved in dichloromethane (205 mL). The aqueous suspension was added to the zirconocene dichloride solution over the course of 5 min, with vigorous stirring. The biphasic mixture was allowed to stir vigorously at room temperature for 30 min. Subsequently, the stir bar was removed, and the mixture was left undisturbed for 24 h. The mixture was filtered through a 350 mL fine sintered glass funnel to collect the white precipitate, which was washed in triplicate with fresh dichloromethane. The solid was dried under reduced pressure at room temperature for 1 h before use. Yield = 3.353 g (79%). ^1H NMR (500 MHz, DMSO-d_6, 25 °C): δ (ppm) = 10.36 (s, μ-OH, 3H), 7.89 (d, benzoate CH, 6H), 7.51 (t, benzoate CH, 3H), 7.37 (t, benzoate CH, 6H), 6.63 (s, Cp, 15H). FTIR (ν, cm^{-1}): 3606, 3168, 1596, 1543, 1495, 1420, 1175, 1018, 815, 716, 614. LTQ-Orbitrap-MS, experimental (calcd) m/z, [M] =

Scheme 1. Ligand Exchange between [ZrCluster]$^+$ and 180° Dicarboxylate Ligands Yields Phase-Pure ZrMOPs[a]

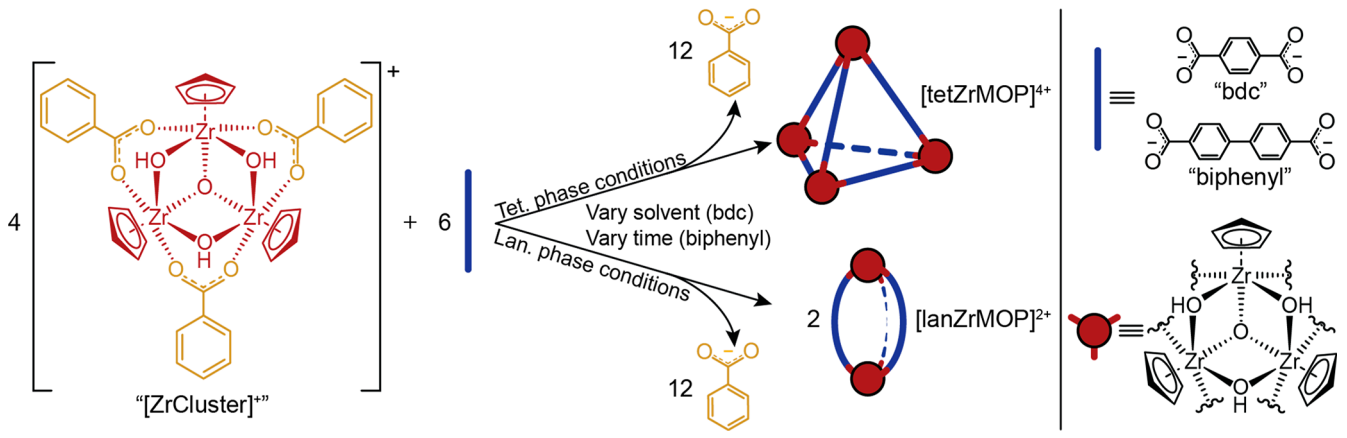

[a]Nodes and ligands are indicated in red and blue, respectively.

https://doi.org/10.1021/acs.chemmater.3c02775
Chem. Mater. 2024, 36, 567−574

$C_{36}H_{33}ClO_{10}Zr_3$: 1832.815 (1832.816) $[2M - Cl^-]^{1+}$, 898.922 (898.923) $[M - Cl^-]^{1+}$.

[ZrCluster]OTf. Care was taken to set up this reaction with the exclusion of light. A solution of silver triflate (350 mg, 1.36 mmol, 1 equiv) in methanol (4 mL) was added to a suspension of [ZrCluster]Cl (1.271 g, 1.36 mmol, 1 equiv) also in methanol (14 mL). The mixture was stirred (400 rpm) in darkness for 48 h, after which it was filtered into a 100 mL RBF. Solvent was removed from the filtrate on a rotary evaporator and/or under dynamic vacuum of a Schlenk line until ∼2 mL of solvent remained. This was decanted and discarded, leaving the product as a white crystalline white solid. Yield = 1.329 g (93%). ^{1}H NMR (500 MHz, DMSO-d_6, 25 °C): δ (ppm) = 10.30 (s, μ-OH, 3H), 7.89 (d, benzoate CH, 6H), 7.51 (t, benzoate CH, 3H), 7.37 (t, benzoate CH, 6H), 6.61 (s, Cp, 15H). ^{19}F{^{1}H} NMR (470 MHz, DMSO-d_6, 25 °C): δ (ppm) = −77.74 (s, OTf). FTIR (ν, cm^{-1}): 3608, 3390, 1594, 1532, 1517, 1404, 1250, 1165, 1019, 808, 720, 610. LTQ-Orbitrap-MS, experimental (calcd) m/z, [M] = $C_{37}H_{33}F_3O_{13}SZr_3$: 1946.799 (1946.800) $[2M - CF_3O_3S^-]^{1+}$, 898.922 (898.923) $[M - CF_3O_3S^-]^{1+}$.

ZrMOPs. Tabulated parameters for ZrMOP synthesis can be found in Table S1.

[tetZrMOP-bdc]Cl$_4$. Terephthalic acid (73.3 mg, 0.441 mmol, 1.65 equiv) was dissolved in DMF (6 mL). The solution was added to a 20 mL vial containing [ZrCluster]Cl (250 mg, 0.267 mmol, 1 equiv) with a stir bar. An additional 1.5 mL of DMF was used to rinse the terephthalic acid solution container and was added to the reaction mixture (7.5 mL total). The mixture was sonicated for 30−60 s until [ZrCluster]Cl was well suspended. The mixture was stirred (150 rpm) at 60 °C for 22 h, after which it was filtered and washed three times with DMF and three times with acetone. The white solid was transferred into a vial and was dried under reduced pressure at room temperature for 1 h. Yield = 183 mg (84%). ^{1}H NMR (500 MHz, DMSO-d_6, 25 °C): δ (ppm) = 10.53 (s, μ-OH, 11H), 7.95 (s, 1,4-bdc CH, 24H), 6.63 (s, Cp, 60H). FTIR (ν, cm^{-1}): 3108, 1668, 1659, 1558, 1506, 1397, 1018, 811, 746, 613, 550. LTQ-Orbitrap-MS, experimental (calcd) m/z, [M] = $C_{108}H_{96}Cl_4O_{40}Zr_{12}$: 1562.701 (1562.699) $[M - 4Cl^- - 2H^+]^{2+}$, 1042.135 (1042.135) $[M - 4Cl^- - H^+]^{3+}$, 781.853 (781.853) $[M - 4Cl^-]^{4+}$.

[tetZrMOP-bdc]OTf$_4$. DMF was dried over 3 Å sieves for 24 h before use to prevent phase separation upon addition to diethyl ether. Terephthalic acid (65.4 mg, 0.393 mmol, 1.65 equiv) was dissolved in DMF (3 mL). [ZrCluster]OTf (250 mg, 0.238 mmol, 1 equiv) was dissolved in DMF (2 mL) in a 20 mL vial with a stir bar. The ligand solution was added to a 20 mL vial with [ZrCluster]OTf solution. An additional 2.5 mL of DMF was used to rinse the terephthalic acid solution container and was added to the reaction mixture (7.5 mL total). The solution was stirred (150 rpm) at 50 °C for 1 h and 15 min. Subsequently, the reaction solution was cooled to room temperature before it was added dropwise to stirring, chilled diethyl ether (60 mL, ∼5 °C), yielding a white precipitate. The mixture was centrifuged and decanted. The resulting white solid was washed three times with diethyl ether and dried under reduced pressure at room temperature for 1 h. Yield = 175 mg (79%). ^{1}H NMR (500 MHz, DMSO-d_6, 25 °C): δ (ppm) = 10.47 (s, μ-OH, 12H), 7.95 (s, 1,4-bdc CH, 24H), 6.60 (s, Cp, 60H). ^{19}F{^{1}H} NMR (470 MHz, DMSO-d_6, 25 °C): δ (ppm) = −77.74 (s, OTf). FTIR (ν, cm^{-1}): 3334, 1652, 1557, 1506, 1398, 1288, 1245, 1160, 1018, 812, 747, 613, 550. LTQ-Orbitrap-MS, experimental (calcd) m/z, [M] = $C_{112}H_{96}O_{52}Zr_{12}S_4F_{12}$: 1712.695 (1712.659) $[M - 2OTf^-]^{2+}$, 1637.714 (1637.679) $[M - 3OTf^- - H^+]^{2+}$, 1562.733 (1562.699) $[M - 4OTf^- - 2H^+]^{2+}$, 1092.145 (1092.122) $[M - 3OTf^-]^{3+}$, 1042.157 (1042.135) $[M - 4OTf^- - H^+]^{3+}$, 781.869 (781.853) $[M - 4OTf^-]^{4+}$.

[lanZrMOP-bdc]Cl$_2$. Terephthalic acid (73.3 mg, 0.441 mmol, 1.65 equiv) was dissolved in DMF (5 mL). H_2O (2.0 mL) was added dropwise while stirring. The solution was added to a 20 mL vial containing [ZrCluster]Cl (250 mg, 0.267 mmol, 1 equiv) with a stir bar. An additional 0.5 mL of DMF was used to rinse the terephthalic acid solution container and was added to the reaction mixture (7.5 mL total). The mixture was sonicated for 30−60 s until [ZrCluster]Cl was well suspended. The mixture was stirred (150 rpm) at 60 °C for 22 h, after which it was filtered and washed three times with DMF and three times with acetone (∼5 mL per wash). The white solid was transferred into a vial and was dried under reduced pressure at room temperature for 1 h. Yield = 137 mg (63%). ^{1}H NMR (500 MHz, DMSO-d_6, 25 °C): δ (ppm) = 10.42 (s, μ-OH, 6H), 7.72 (s, 1,4-bdc CH, 12H), 6.65 (s, Cp, 30H). FTIR (ν, cm^{-1}): 3615, 3190, 1653, 1543, 1532, 1408, 1100, 1018, 810, 748, 604, 593. LTQ-Orbitrap-MS, experimental (calcd) m/z, [M] = $C_{54}H_{48}Cl_2O_{20}Zr_6$: 1599.676 (1599.675) $[2M - 2Cl^-]^{2+}$, 1562.700 (1562.699) $[M - 2Cl^- - H^+]^{1+}$, 781.853 (781.853) $[M - 2Cl^-]^{2+}$.

[lanZrMOP-bdc]OTf$_2$. Care was taken to set up this reaction in the absence of light. A solution of silver triflate (51.8 mg, 0.202 mmol, 2.2 equiv) in methanol (2.0 mL) was added to a suspension of [lanZrMOP-bdc]Cl$_2$ (150 mg, 0.092 mmol, 1 equiv) in methanol (5.5 mL). The mixture was stirred (200 rpm) in darkness for 25 h. The resulting purple suspension was filtered through Celite into a 100 mL RBF. Solvent was removed from the clear, colorless filtrate on a rotary evaporator and/or under dynamic vacuum of a Schlenk line leaving the product as a white solid. Yield = 118 mg (69%). ^{1}H NMR (500 MHz, DMSO-d_6, 25 °C): δ (ppm) = 10.37 (s, μ−OH, 6H), 7.72 (s, 1,4-bdc CH, 12H), 6.63 (s, Cp, 30H). ^{19}F{^{1}H} NMR (470 MHz, DMSO-d_6, 25 °C): δ (ppm) = −77.74 (s, OTf). FTIR (ν, cm^{-1}): 3404, 1660, 1547, 1505, 1411, 1258, 1170, 1020, 812, 747, 602. LTQ-Orbitrap-MS, experimental (calcd) m/z, [M] = 1712.694 (1712.658) $[M - OTf^-]^{1+}$, 781.869 (781.853) $[M - 2OTf^-]^{2+}$.

[tetZrMOP-biphenyl]OTf$_4$. DMF was dried over 3 Å sieves for 24 h before use to prevent phase separation upon addition to diethyl ether. [ZrCluster]OTf (350 mg, 0.334 mmol, 1 equiv) was dissolved in DMF (5 mL). The solution was added to a 20 mL vial containing biphenyl-4,4′-dicarboxylic acid (133.4 mg, 0.551 mmol, 1.65 equiv) suspended in DMF (7 mL) with a stir bar. An additional 2 mL of DMF was used to rinse the [ZrCluster]OTf solution container and was added to the reaction mixture (14 mL total). The mixture was stirred (220 rpm) at 50 °C for 20 min. Subsequently, the reaction solution was cooled to room temperature before it was added dropwise to stirring, chilled diethyl ether (90 mL, ∼5 °C), yielding a white precipitate. The mixture was centrifuged, and the supernatant was decanted. The resulting white solid (crude product, 278 mg) was washed once with diethyl ether and dried under reduced pressure at room temperature for 5 min. The solid was then redissolved in methanol (30 mL) and added dropwise to room temperature diethyl ether (75 mL). The mixture was centrifuged, and the supernatant was decanted. The resulting white solid was washed three times with diethyl ether and dried under reduced pressure at room temperature for 30 min. Yield = 193 mg (55%). ^{1}H NMR (500 MHz, DMSO-d_6, 25 °C): δ (ppm) = 10.48 (s, μ−OH, 12H), 7.96 (d, biphenyl CH, 24H), 7.88 (d, biphenyl CH, 24H), 6.64 (s, Cp, 60H). ^{19}F{^{1}H} NMR (470 MHz, DMSO-d_6, 25 °C): δ (ppm) = −77.74 (s, OTf). FTIR (ν, cm^{-1}): 3162, 1660, 1535, 1528, 1410, 1245, 1181, 1019, 812, 770, 676, 612. LTQ-Orbitrap-MS, experimental (calcd) m/z, [M] = $C_{148}H_{120}O_{52}Zr_{12}S_4F_{12}$: 1866.324 (1866.273) $[M - 3OTf^- - H^+]^{2+}$, 1791.340 (1791.294) $[M - 4OTf^- - 2H^+]^{2+}$, 1244.553 (1244.518) $[M - 3OTf^-]^{3+}$, 1194.565 (1194.531) $[M - 4OTf^- - H^+]^{3+}$, 896.175 (896.150) $[M - 4OTf^-]^{4+}$.

[lanZrMOP-biphenyl]OTf$_2$. DMF was dried over 3 Å sieves for 24 h before use to prevent phase separation upon addition to diethyl ether. [ZrCluster]OTf (250 mg, 0.238 mmol, 1 equiv) was dissolved in DMF (6 mL). The solution was added to a 20 mL vial containing biphenyl-4,4′-dicarboxylic acid (95.3 mg, 0.393 mmol, 1.65 equiv) with a stir bar. An additional 1.5 mL of DMF was used to rinse the [ZrCluster]OTf solution container and was added to the reaction mixture (7.5 mL total). The mixture was sonicated for 30−60 s until biphenyl-4,4′-dicarboxylic acid was well suspended. The mixture was stirred (220 rpm) at 60 °C for 20 h. Subsequently, the reaction solution was cooled to room temperature before it was added dropwise to stirring, chilled diethyl ether (60 mL, ∼5 °C), yielding a white precipitate. The mixture was centrifuged, and the supernatant was decanted. The resulting white solid was washed three times with diethyl ether and dried under reduced pressure at room temperature for 1 h. Yield = 163 mg (65%). ^{1}H NMR (500 MHz, DMSO-d_6, 25

https://doi.org/10.1021/acs.chemmater.3c02775
Chem. Mater. 2024, 36, 567−574

°C): δ (ppm) = 10.27 (s, μ-OH, 6H), 7.62 (d, biphenyl CH, 12H), 7.36 (d, biphenyl CH, 12H), 6.65 (s, Cp, 30H). $^{19}F\{^1H\}$ NMR (470 MHz, DMSO-d_6, 25 °C): δ (ppm) = −77.74 (s, OTf). FTIR (ν, cm^{-1}): 3340, 1652, 1575, 1520, 1412, 1256, 1241, 1164, 1030, 811, 769, 609. LTQ-Orbitrap-MS, experimental (calcd) m/z, [M] = $C_{74}H_{60}F_6O_{26}S_2Zr_6$: 1940.755 (1940.753) $[M - CF_3O_3S^-]^{1+}$, 1790.795 (1790.793) $[M - 2CF_3O_3S^- - H^+]^{1+}$, 895.900 (895.900) $[M - 2CF_3O_3S^-]^{2+}$.

RESULTS AND DISCUSSION

Synthetic Methods. We have established that [ZrCluster]$^+$ can be used as a general precursor for the formation of architectures containing Cp-capped Zr nodes. This approach works for both Cl^- and OTf^- counterions. We found that subsequent ligand exchange occurred readily under a variety of conditions, including when both reactants were soluble (e.g., [ZrCluster]OTf with 1,4-benzenedicarboxylic acid), when one of two reactants was soluble (e.g., [ZrCluster]OTf with biphenyl-4,4′-dicarboxylic acid and [ZrCluster]Cl with 1,4-benzenedicarboxylic acid), and when both reactants were poorly soluble (e.g., [ZrCluster]Cl with biphenyl-4,4′-dicarboxylic acid). In the latter case, though, we were unable to make a phase-pure material regardless of the reaction time, temperature, or solvent. Thus, conditions under which one or both reactants were soluble were explored further.

For [tetZrMOP-bdc]Cl_4, high yields of phase-pure tetrahedron were achieved using DMF as a reaction solvent and allowing the reaction to run for 22 h at 60 °C. With a simple addition of water to the reaction, leaving all other conditions unchanged, a complete change in synthetic outcome to [lanZrMOP-bdc]Cl_2 was achieved. Similar conditions were used to isolate the phase-pure [tetZrMOP-bdc]OTf_4. Interestingly, the addition of water does not change the synthetic outcome when starting with [ZrCluster]OTf, and only [tetZrMOP-bdc]OTf_4 was obtained. However, we are able to form phase-pure [lanZrMOP-bdc]OTf_2 by a postsynthetic counterion exchange on [lanZrMOP-bdc]Cl_2 with no scrambling of phase occurring.

Recent work has suggested that ZrMOP tetrahedra are kinetic products, while lanterns are thermodynamically favored, in certain conditions.[24,48] This feature was exploited to isolate phase-pure [ZrMOP-biphenyl]OTf_X materials, where [tetZrMOP-biphenyl]OTf_4 was isolated with a reaction time of only 20 min, and lanterns were present with any reaction time >30 min. To isolate phase-pure [lanZrMOP-biphenyl]OTf_2 in good yields, the reaction was allowed to run for 20 h. The reason that the addition of water was not used to control phase purity in this system is that the biphenyl ligand is poorly soluble even in DMF, and in water/DMF mixtures, the solubility is even lower to the extent that self-assembly is hindered.

In the cases of [ZrMOP]Cl_X products, isolation of the white solid directly from the reaction mixture followed by washes with DMF/acetone consistently yielded pure products. Because of the enhanced solubility of the [ZrMOP]OTf_X products, the reaction mixtures were added to diethyl ether to precipitate the crude products as white solids. In most cases, this yielded pure product. Otherwise, dissolving in methanol and reprecipitating into diethyl ether was used to purify further.

NMR and Mass Spectrometry. For NMR characterization (Figures S1−S21), DMSO-d_6 is preferred over a protic solvent (e.g., MeOD) to maintain observable μ-OH resonances that are useful for discriminating between structures. The use of protic solvents may result in the loss of valuable information, especially in the cases of ZrMOP-bdc where a ligand resonance may be mistaken for residual DMF. Across different bridging ligands and counterions, the μ-OH and aromatic ligand resonances of lanterns are consistently shifted upfield of their tetrahedral analogues in ^1H NMR spectra (Figure 2). The location of the cyclopentadienyl ^1H resonance remains largely unchanged across ZrMOP architectures.

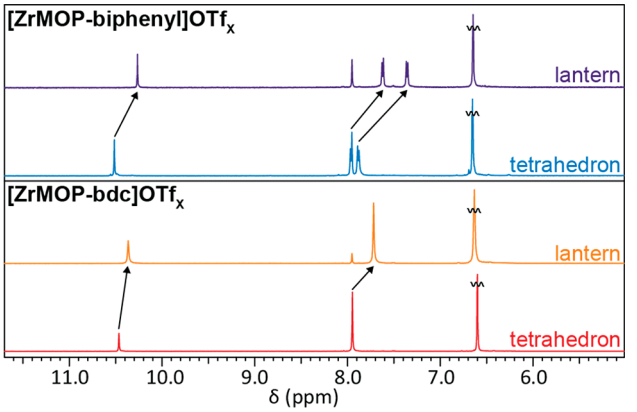

Figure 2. ^1H NMR spectra of [ZrMOP-bdc]OTf_X and [ZrMOP-biphenyl]OTf_X, where X = 2 for lanterns and 4 for tetrahedra. Shifts in μ-OH and ligand resonances between the two architectures are emphasized with arrows.

The aromatic peaks of free ligands are within 0.1 ppm of their analogous resonance as part of a tetrahedron, but the same resonance is shifted between 0.3 and 0.5 ppm when they are in a lantern. For example, the ^1H NMR of biphenyl-4,4′-dicarboxylic acid (DMSO-d_6, 25 °C) has two doublets at 8.05 and 7.87 ppm, appearing quite similar to the peaks of [tetZrMOP-biphenyl]OTf_4 at 7.96 and 7.88 ppm (Figure S16). These can be compared to the peaks of [lanZrMOP-biphenyl]OTf_2 at 7.62 and 7.36 ppm (Figure S19), which are shifted further from the free ligand, and the two protons are now 0.26 ppm separated rather than 0.08 ppm. This suggests that the ^1H environments of these ligands are more perturbed in lantern architectures than in tetrahedra.

Two-dimensional diffusion ordered spectroscopy (DOSY) NMR (Figures S7, S10, S12, S15, S18, and S21) was used to confirm the phase purity of ZrMOP materials and was especially useful in cases where ^1H NMR alone may be ambiguous. For example, [lanZrMOP-bdc]Cl_2 has a ligand resonance at 7.72 ppm, along with a peak at 7.95 ppm which could be either residual DMF or [tetZrMOP-bdc]Cl_4 (Figures S11 and S12). DOSY NMR shows that the peak at 7.95 ppm diffuses as a solvent, and this is further supported by the ^1H NMR integrations of the three DMF resonances (7.95, 2.89, and 2.73 ppm), confirming that [lanZrMOP-bdc]Cl_2 is phase-pure. Furthermore, DOSY diffusion coefficients were used to compare hydrodynamic radii of tetrahedra and lanterns through the Stokes−Einstein equation.[58] Diffusion coefficients of μ-OH resonances were not considered because residual H_2O enables proton exchange, resulting in skewed diffusion coefficients. Tetrahedra consistently had hydrodynamic radii 0.5 nm larger than their lantern analogues (Tables S2 and S3), establishing DOSY is a useful technique to determine phase-

https://doi.org/10.1021/acs.chemmater.3c02775
Chem. Mater. 2024, 36, 567−574

purity of ZrMOP mixtures and distinguish tetrahedra from lanterns.

Mass spectrometry also proved to be useful in discriminating between tetrahedra and lanterns (Figures S22–S29). Although the 4+ and 2+ m/z values of tetrahedra are common with the 2+ and 1+, respectively, of lanterns, the lack of a 3+ peak is strong evidence that a phase-pure lantern is present (Figure 3).

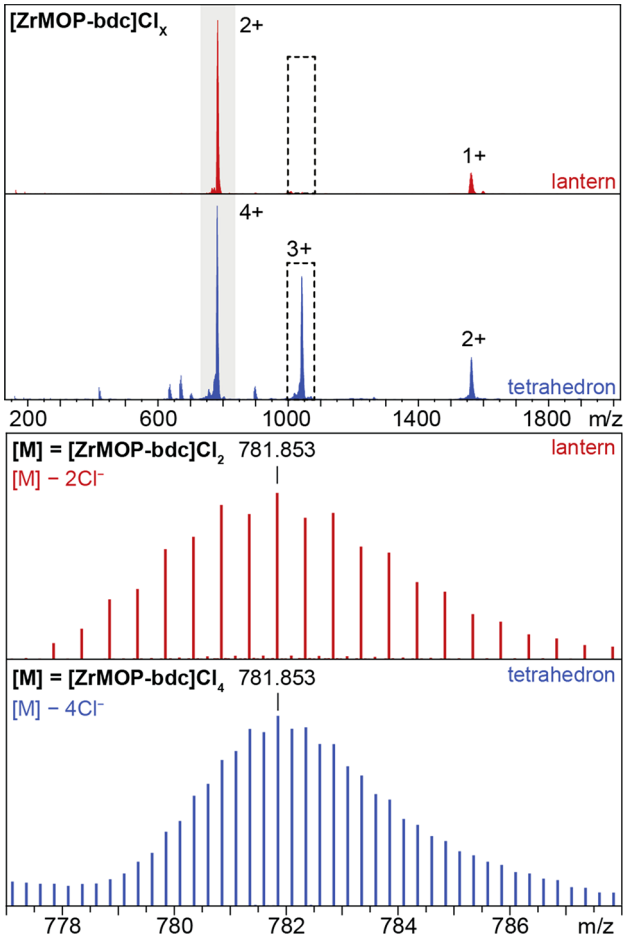

Figure 3. Top: full mass spectra of [ZrMOP-bdc]Cl$_X$ as a tetrahedron (X = 4) and a lantern (X = 2). The lack of a 3+ peak in the lantern architecture is highlighted (dashed box). Bottom: the 4+ and 2+ peaks shown in detail so the unique peak spacing can be observed.

The presence of a 3+ peak, though, is not enough to confirm phase-pure tetrahedra because a mixture may be present. The peak spacing and isotopic distribution of the 4+/2+ peaks was used for this, as any lantern present as a mixture will result in diagnostic changes to the relative peak intensities.

Brunauer–Emmett–Teller (BET) Areas and Materials Characterization. Nitrogen sorption isotherms were collected for all samples at 77 K after activating them at 60 °C under vacuum (Figures S39–S44A). Powder X-ray diffraction (PXRD) patterns collected before activation and after nitrogen sorption measurements indicated that the selected activation conditions and the adsorption measurements did not alter the cage packing of the sample (Figure S48). Brunauer–Emmett–Teller (BET) areas for the ZrMOPs were calculated using the adsorption isotherms based on the consistency criteria reported by Rouquerol et al.[59] BET areas calculated for the tetrahedral geometries are orders of magnitude higher than the ones calculated for the lanterns (Table 1). Interestingly, this

Table 1. BET Areas of Tetrahedral and Lantern ZrMOPs (X = 4 for Tetrahedra and X = 2 for Lanterns)

	BET area (m^2/g)	
MOP type	tetrahedron	lantern
[ZrMOP-bdc]Cl$_X$	462.5	12.9
[ZrMOP-bdc]OTf$_X$	392.8	20.0
[ZrMOP-biphenyl]OTf$_X$	605.2	4.2

trend is observed with all six MOPs irrespective of the ligand or the counterion. BET plots and Rouquerol plots for all MOPs are provided (Figures S39–S44). The lower BET areas of the lanterns is attributed to the absence of any significant internal cavity as these architectures have three parallel dicarboxylate donors. The small internal volume that may be present is inaccessible to the carrier gas. This explanation is further supported by pore size distribution (PSD) measurements. Pore sizes on the order of what may be expected for the intrinsic porosity of MOPs were observed only for the tetrahedral structures (Figures S45–S47). PXRD data show sharp crystalline peaks for the lanterns in contrast to the more amorphous peak pattern shown by the tetrahedra (Figure S48). The TGA curves for all phase-pure materials are provided in Figures S31–S38.

CONCLUSIONS

Benzoate-capped ZrClusters with both chloride and triflate counterions were shown to undergo ligand exchange with 1,4-benzenedicarboxylate and 4,4′-biphenyldicarboxylate ligands to form ZrMOPs. Phase-pure materials were obtained by modifying reaction conditions, including solvent, reaction time, and reaction temperature. This new approach to ZrMOP synthesis where node formation is separated from the self-assembly step is an important tool to generate single architectures, especially because traditional methods often result in inseparable mixtures. Furthermore, this approach can also enable the use of ligands that are incompatible with common ZrMOP self-assembly conditions, for example, ligands that react with the water required to form the Zr nodes or ligands that will react with the exogenous cyclopentadiene that is formed as a side product. The resulting lanterns and tetrahedra were fully characterized and shown to have unique ^{1}H/DOSY NMR and mass spectra, establishing that these techinques can be used to assess phase purity.

This new route to phase-pure ZrMOPs maintains the attractive tunability of these materials where a broad library of ligands may be used and enhances studies of structure–function relationships by eliminating the complexities associated with analyzing mixtures. We demonstrate this using surface area measurements, where the high surface area of the material is attributed to only a single phase. Specifically, tetrahedra have significantly larger surface areas than lanterns, and this general trend was shown to be independent of the counterion and ligand. Because many applications of MOPs are predicated on their permanent porosity, establishing general routes to phase-pure materials with unique physicochemical properties will enhance their use as stand-alone materials or as components of hybrids or composites.

ASSOCIATED CONTENT

Supporting Information

The Supporting Information is available free of charge at https://pubs.acs.org/doi/10.1021/acs.chemmater.3c02775.

https://doi.org/10.1021/acs.chemmater.3c02775
Chem. Mater. 2024, 36, 567–574

$^{1}H/^{19}F$/DOSY NMR spectra, mass spectra, FTIR spectra, TGA data, nitrogen adsorption isotherms, BET plots, and Rouquerol plots (PDF)

AUTHOR INFORMATION

Corresponding Author

Timothy R. Cook − *Department of Chemistry, University at Buffalo, the State University of New York, Buffalo, New York 14260-3000, United States;* orcid.org/0000-0002-7668-8089; Email: trcook@buffalo.edu

Authors

Meghan G. Sullivan − *Department of Chemistry, University at Buffalo, the State University of New York, Buffalo, New York 14260-3000, United States;* orcid.org/0000-0002-0862-3072

Heshali K. Welgama − *Department of Chemistry, University at Buffalo, the State University of New York, Buffalo, New York 14260-3000, United States;* orcid.org/0000-0002-9826-9803

Matthew R. Crawley − *Department of Chemistry, University at Buffalo, the State University of New York, Buffalo, New York 14260-3000, United States;* orcid.org/0000-0002-2555-9543

Alan E. Friedman − *Department of Chemistry, University at Buffalo, the State University of New York, Buffalo, New York 14260-3000, United States;* orcid.org/0000-0002-4764-8168

Complete contact information is available at: https://pubs.acs.org/10.1021/acs.chemmater.3c02775

Author Contributions

M.G.S. conducted experimental/synthetic work, collected $^{1}H/DOSY/^{19}F$ NMR, MS, TGA, and FTIR data, wrote the main text, and contributed to conceptualization, investigation, and data curation. H.K.W. conducted surface area measurements with corresponding data analysis and contributed to conceptualization and writing of surface area discussion. M.R.C conducted powder X-ray data collection and analysis. A.E.F. was responsible for collecting mass spectrometry data. T.R.C. contributed to conceptualization, project administration, resources, funding acquisition, supervision, and writing−review/editing.

Notes

The authors declare no competing financial interest.

ACKNOWLEDGMENTS

This work was supported by the Department of Energy (DEFE0031736), NSF 1847950, and NSF 2015723. M.G.S. was supported by the Barry Goldwater Scholarship and Excellence in Education Foundation. Nuclear magnetic resonance experiments were performed in the UB MR Center using the Bruker AVANCE NEO 500 MHz NMR (NSF CHE 2018160). Rigaku XtaLAB Synergy-S, a part of the Chemistry Instrument Center (CIC) at UB, was purchased with NSF CHE-2216151.

REFERENCES

(1) Cook, T. R.; Zheng, Y.-R.; Stang, P. J. Metal-Organic Frameworks and Self-Assembled Supramolecular Coordination Complexes: Comparing and Contrasting the Design, Synthesis, and Functionality of Metal-Organic Materials. *Chem. Rev.* **2013**, *113* (1), 734−777.

(2) McTernan, C. T.; Davies, J. A.; Nitschke, J. R. Beyond Platonic: How to Build Metal-Organic Polyhedra Capable of Binding Low-Symmetry, Information-Rich Molecular Cargoes. *Chem. Rev.* **2022**, *122* (11), 10393−10437.

(3) Lee, S.; Jeong, H.; Nam, D.; Lah, M. S.; Choe, W. The rise of metal-organic polyhedra. *Chem. Soc. Rev.* **2021**, *50* (1), 528−555.

(4) Lin, R.-B.; Xiang, S.; Xing, H.; Zhou, W.; Chen, B. Exploration of porous metal-organic frameworks for gas separation and purification. *Coord. Chem. Rev.* **2019**, *378*, 87−103.

(5) Rodenas, T.; Luz, I.; Prieto, G.; Seoane, B.; Miro, H.; Corma, A.; Kapteijn, F.; Llabrés i Xamena, F. X.; Gascon, J. Metal-organic framework nanosheets in polymer composite materials for gas separation. *Nat. Mater.* **2015**, *14* (1), 48−55.

(6) Jiao, L.; Seow, J. Y. R.; Skinner, W. S.; Wang, Z. U.; Jiang, H.-L. Metal-organic frameworks: Structures and functional applications. *Mater. Today* **2019**, *27*, 43−68.

(7) Siegelman, R. L.; Kim, E. J.; Long, J. R. Porous materials for carbon dioxide separations. *Nat. Mater.* **2021**, *20* (8), 1060−1072.

(8) Jiao, L.; Wang, Y.; Jiang, H.-L.; Xu, Q. Metal-Organic Frameworks as Platforms for Catalytic Applications. *Adv. Mater.* **2018**, *30* (37), 1703663.

(9) Dhakshinamoorthy, A.; Li, Z.; Garcia, H. Catalysis and photocatalysis by metal organic frameworks. *Chem. Soc. Rev.* **2018**, *47* (22), 8134−8172.

(10) Oldacre, A. N.; Friedman, A. E.; Cook, T. R. A Self-Assembled Cofacial Cobalt Porphyrin Prism for Oxygen Reduction Catalysis. *J. Am. Chem. Soc.* **2017**, *139* (4), 1424−1427.

(11) Xia, J.; Gao, Y.; Yu, G. Tetracycline removal from aqueous solution using zirconium-based metal-organic frameworks (Zr-MOFs) with different pore size and topology: Adsorption isotherm, kinetic and mechanism studies. *J. Colloid Interface Sci.* **2021**, *590*, 495−505.

(12) Ahmadijokani, F.; Molavi, H.; Rezakazemi, M.; Tajahmadi, S.; Bahi, A.; Ko, F.; Aminabhavi, T. M.; Li, J.-R.; Arjmand, M. UiO-66 metal-organic frameworks in water treatment: A critical review. *Prog. Mater. Sci.* **2022**, *125*, 100904.

(13) Jun, B.-M.; Al-Hamadani, Y. A. J.; Son, A.; Park, C. M.; Jang, M.; Jang, A.; Kim, N. C.; Yoon, Y. Applications of metal-organic framework based membranes in water purification: A review. *Sep. Purif. Technol.* **2020**, *247*, 116947.

(14) Drout, R. J.; Robison, L.; Chen, Z.; Islamoglu, T.; Farha, O. K. Zirconium Metal-Organic Frameworks for Organic Pollutant Adsorption. *Trends Chem.* **2019**, *1* (3), 304−317.

(15) Cook, T. R.; Vajpayee, V.; Lee, M. H.; Stang, P. J.; Chi, K.-W. Biomedical and Biochemical Applications of Self-Assembled Metallacycles and Metallacages. *Acc. Chem. Res.* **2013**, *46* (11), 2464−2474.

(16) Sokolow, G. E.; Crawley, M. R.; Morphet, D. R.; Asik, D.; Spernyak, J. A.; McGray, A. J. R.; Cook, T. R.; Morrow, J. R. Metal-Organic Polyhedron with Four Fe(III) Centers Producing Enhanced T1Magnetic Resonance Imaging Contrast in Tumors. *Inorg. Chem.* **2022**, *61* (5), 2603−2611.

(17) Lewis, J. E. M.; Gavey, E. L.; Cameron, S. A.; Crowley, J. D. Stimuli-responsive Pd2L4 metallosupramolecular cages: towards targeted cisplatin drug delivery. *Chem. Sci.* **2012**, *3* (3), 778−784.

(18) Vajpayee, V.; Song, Y. H.; Yang, Y. J.; Kang, S. C.; Kim, H.; Kim, I. S.; Wang, M.; Stang, P. J.; Chi, K.-W. Coordination-Driven Self-Assembly and Anticancer Activity of Molecular Rectangles Containing Octahedral Ruthenium Metal Centers. *Organometallics* **2011**, *30* (12), 3242−3245.

(19) Zhang, H.; Liu, X.; Wu, Y.; Guan, C.; Cheetham, A. K.; Wang, J. MOF-derived nanohybrids for electrocatalysis and energy storage: current status and perspectives. *Chem. Commun.* **2018**, *54* (42), 5268−5288.

(20) Du, R.; Wu, Y.; Yang, Y.; Zhai, T.; Zhou, T.; Shang, Q.; Zhu, L.; Shang, C.; Guo, Z. Porosity Engineering of MOF-Based Materials for Electrochemical Energy Storage. *Adv. Energy Mater.* **2021**, *11* (20), 2100154.

(21) Pastore, V. J.; Sullivan, M. G.; Welgama, H. K.; Crawley, M. R.; Friedman, A. E.; Rumsey, C.; Trebbin, M.; Rzayev, J.; Cook, T. R. Clickable Norbornene-Based Zirconium Carboxylate Polyhedra. *Chem. Mater.* **2023**, *35* (4), 1651−1658.
(22) Burtch, N. C.; Jasuja, H.; Walton, K. S. Water Stability and Adsorption in Metal-Organic Frameworks. *Chem. Rev.* **2014**, *114* (20), 10575−10612.
(23) Bae, J.; Choi, J. S.; Hwang, S.; Yun, W. S.; Song, D.; Lee, J.; Jeong, N. C. Multiple Coordination Exchanges for Room-Temperature Activation of Open-Metal Sites in Metal-Organic Frameworks. *ACS Appl. Mater. Interfaces* **2017**, *9* (29), 24743−24752.
(24) Sullivan, M. G.; Sokolow, G. E.; Jensen, E. T.; Crawley, M. R.; MacMillan, S. N.; Cook, T. R. Altering the solubility of metal-organic polyhedra via pendant functionalization of Cp3Zr3O(OH)3 nodes. *Dalton Trans.* **2023**, *52* (2), 338−346.
(25) Liu, G.; Ju, Z.; Yuan, D.; Hong, M. In Situ Construction of a Coordination Zirconocene Tetrahedron. *Inorg. Chem.* **2013**, *52* (24), 13815−13817.
(26) Liu, G.; Di Yuan, Y.; Wang, J.; Cheng, Y.; Peh, S. B.; Wang, Y.; Qian, Y.; Dong, J.; Yuan, D.; Zhao, D. Process-Tracing Study on the Postassembly Modification of Highly Stable Zirconium Metal-Organic Cages. *J. Am. Chem. Soc.* **2018**, *140* (20), 6231−6234.
(27) Jiang, Y.; Tan, P.; Qi, S.-C.; Gu, C.; Peng, S.-S.; Wu, F.; Liu, X.-Q.; Sun, L.-B. Breathing Metal-Organic Polyhedra Controlled by Light for Carbon Dioxide Capture and Liberation. *CCS Chem.* **2021**, *3* (6), 1659−1668.
(28) El-Sayed, E.-S. M.; Yuan, Y. D.; Zhao, D.; Yuan, D. Zirconium Metal-Organic Cages: Synthesis and Applications. *Acc. Chem. Res.* **2022**, *55* (11), 1546−1560.
(29) Chen, S.; Cheng, S.; Zhao, L.; Sun, C.; Qin, C.; Su, Z. Self-assembly of zirconocene-based metal-organic capsules: the structure, luminescence sensing of Fe3+ and iodine capture. *New J. Chem.* **2020**, *44* (48), 21255−21260.
(30) Yang, X.; Yu, X.-Y.; Wang, Q.; Zou, J.; Liao, G.-P.; Li, M.-T.; Liu, X.-L.; Xia, H.; Xu, F.-J. Metal-organic cages ZrT-1-NH2 for rapid and selective sensing of nitrite. *Chin. J. Anal. Chem.* **2023**, *51* (2), 100213.
(31) Yang, H.; Li, M.; Cai, Y.; Zhou, M.; Liu, G. Self-Assembly of a Lantern-Like Zirconium Metal-Organic Cage Decorated with μ2-OH Functional Groups for Potential Al3+ Ion Detection. *Cryst. Growth Des.* **2021**, *21* (12), 6642−6647.
(32) Huang, H.; Liu, Z.-Y.; Li, S.-B.; Zhu, J.; Jiang, B.-X.; Zhang, Y.-T. Amino-functionalized Zr (IV) metal-organic polyhedron as water-stable catalyst for the photocatalytic degradation of tetracycline. *J. Solid State Chem.* **2022**, *307*, 122821.
(33) Huang, H.; Xu, T.-T.; Wang, B.-L.; Lv, N.; Zhang, Y.-T. Construction of zirconium metal-organic polyhedron/silver chloride heterojunction with boosted photocatalytic activity for the degradation of broad-spectrum antibiotics and mechanism insight. *Sep. Purif. Technol.* **2023**, *307*, 122848.
(34) Sun, M.; Wang, Q.-Q.; Qin, C.; Sun, C.-Y.; Wang, X.-L.; Su, Z.-M. An Amine-Functionalized Zirconium Metal-Organic Polyhedron Photocatalyst with High Visible-Light Activity for Hydrogen Production. *Eur. J. Chem.* **2019**, *25* (11), 2824−2830.
(35) Tang, J.; Wei, F.; Ding, S.; Wang, X.; Xie, G.; Fan, H. Azo-Functionalized Zirconium-Based Metal-Organic Polyhedron as an Efficient Catalyst for CO_2 Fixation with Epoxides. *Eur. J. Chem.* **2021**, *27* (50), 12890−12899.
(36) Kim, S.; Jee, S.; Choi, K. M.; Shin, D.-S. Single-atom Pd catalyst anchored on Zr-based metal-organic polyhedra for Suzuki-Miyaura cross coupling reactions in aqueous media. *Nano Res.* **2021**, *14* (2), 486−492.
(37) Delgado, P.; Martin-Romera, J. D.; Perona, C.; Vismara, R.; Galli, S.; Maldonado, C. R.; Carmona, F. J.; Padial, N. M.; Navarro, J. A. R. Zirconium Metal-Organic Polyhedra with Dual Behavior for Organophosphate Poisoning Treatment. *ACS Appl. Mater. Interfaces* **2022**, *14* (23), 26501−26506.
(38) Li, Y.; Dong, J.; Gong, W.; Tang, X.; Liu, Y.; Cui, Y.; Liu, Y. Artificial Biomolecular Channels: Enantioselective Transmembrane Transport of Amino Acids Mediated by Homochiral Zirconium Metal-Organic Cages. *J. Am. Chem. Soc.* **2021**, *143* (49), 20939−20951.
(39) Liu, J.; Duan, W.; Song, J.; Guo, X.; Wang, Z.; Shi, X.; Liang, J.; Wang, J.; Cheng, P.; Chen, Y.; et al. Self-Healing Hyper-Cross-Linked Metal-Organic Polyhedra (HCMOPs) Membranes with Antimicrobial Activity and Highly Selective Separation Properties. *J. Am. Chem. Soc.* **2019**, *141* (30), 12064−12070.
(40) Cheng, S.; Chen, W.; Zhao, L.; Wang, X.; Qin, C.; Su, Z. Synthesis, crystal structure and iodine capture of Zr-based metal-organic polyhedron. *Inorg. Chim. Acta* **2021**, *516*, 120174.
(41) Fan, W.; Peh, S. B.; Zhang, Z.; Yuan, H.; Yang, Z.; Wang, Y.; Chai, K.; Sun, D.; Zhao, D. Tetrazole-Functionalized Zirconium Metal-Organic Cages for Efficient C2H2/C2H4 and C2H2/CO_2 Separations. *Angew. Chem., Int. Ed.* **2021**, *60* (32), 17338−17343.
(42) Yang, Z.; Liu, G.; Yuan, Y. D.; Peh, S. B.; Ying, Y.; Fan, W.; Yu, X.; Yang, H.; Wu, Z.; Zhao, D. Homoporous hybrid membranes containing metal-organic cages for gas separation. *J. Membr. Sci.* **2021**, *636*, 119564.
(43) Yang, Z.; Wu, Z.; Peh, S. B.; Ying, Y.; Yang, H.; Zhao, D. Mixed-Matrix Membranes Containing Porous Materials for Gas Separation: From Metal-Organic Frameworks to Discrete Molecular Cages. *Engineering* **2023**, *23*, 40−55.
(44) Qin, L.-Z.; Xiong, X.-H.; Wang, S.-H.; Meng, L.-L.; Yan, T.-A.; Chen, J.; Zhu, N.-X.; Liu, D.-H.; Wei, Z.-W. A Series of Functionalized Zirconium Metal-Organic Cages for Efficient CO_2/N2 Separation. *Inorg. Chem.* **2021**, *60* (23), 17440−17444.
(45) Xing, W.-H.; Li, H.-Y.; Dong, X.-Y.; Zang, S.-Q. Robust multifunctional Zr-based metal-organic polyhedra for high proton conductivity and selective CO_2 capture. *J. Mater. Chem. A* **2018**, *6* (17), 7724−7730.
(46) Gosselin, A. J.; Decker, G. E.; McNichols, B. W.; Baumann, J. E.; Yap, G. P. A.; Sellinger, A.; Bloch, E. D. Ligand-Based Phase Control in Porous Zirconium Coordination Cages. *Chem. Mater.* **2020**, *32* (13), 5872−5878.
(47) Chen, X.; Li, S.-B.; Liu, Z.-Y.; Zhang, Y.-T. Solvent-directed assembly of Zr-based metal-organic cages for dye adsorption from aqueous solution. *J. Solid State Chem.* **2021**, *296*, 121998.
(48) Xiao, Z.; Drake, H. F.; Rezenom, Y. H.; Cai, P.; Zhou, H.-C. Structural Manipulation of a Zirconocene-Based Porous Coordination Cage Using External and Host-Guest Stimuli. *Small Structures* **2022**, *3* (5), 2100133.
(49) Pastore, V. J.; Sullivan, M. G.; Rzayev, J.; Cook, T. R. Postsynthetic polymer-ligand exchange hybridization in M-MOF-74 composites. *J. Coord. Chem.* **2021**, *74* (1−3), 178−189.
(50) Pastore, V. J.; Cook, T. R.; Rzayev, J. Polymer-MOF Hybrid Composites with High Porosity and Stability through Surface-Selective Ligand Exchange. *Chem. Mater.* **2018**, *30* (23), 8639−8649.
(51) Chiu, C.-C.; Shieh, F.-K.; Tsai, H.-H. G. Ligand Exchange in the Synthesis of Metal-Organic Frameworks Occurs Through Acid-Catalyzed Associative Substitution. *Inorg. Chem.* **2019**, *58* (21), 14457−14466.
(52) Jerozal, R. T.; Pitt, T. A.; MacMillan, S. N.; Milner, P. J. High-Concentration Self-Assembly of Zirconium- and Hafnium-Based Metal-Organic Materials. *J. Am. Chem. Soc.* **2023**, *145* (24), 13273−13283.
(53) Decker, G. E.; Lorzing, G. R.; Deegan, M. M.; Bloch, E. D. MOF-mimetic molecules: carboxylate-based supramolecular complexes as molecular metal-organic framework analogues. *J. Mater. Chem. A* **2020**, *8* (8), 4217−4229.
(54) Kalaj, M.; Prosser, K. E.; Cohen, S. M. Room temperature aqueous synthesis of UiO-66 derivatives via postsynthetic exchange. *Dalton Trans.* **2020**, *49* (26), 8841−8845.
(55) Kim, M.; Cahill, J. F.; Su, Y.; Prather, K. A.; Cohen, S. M. Postsynthetic ligand exchange as a route to functionalization of 'inert' metal-organic frameworks. *Chem. Sci.* **2012**, *3* (1), 126−130.
(56) Winarta, J.; Shan, B.; McIntyre, S. M.; Ye, L.; Wang, C.; Liu, J.; Mu, B. A Decade of UiO-66 Research: A Historic Review of Dynamic Structure, Synthesis Mechanisms, and Characterization Techniques of

an Archetypal Metal-Organic Framework. *Cryst. Growth Des.* **2020**, *20* (2), 1347−1362.
(57) Iden, H.; Bi, W.; Morin, J.-F.; Fontaine, F.-G. Zirconium(IV) Metallocavitands As Blue-Emitting Materials. *Inorg. Chem.* **2014**, *53* (6), 2883−2891.
(58) Lv, Z.; Yu, C.; Zhu, X.; Wang, Y. Virus-like Cage Hybrid: Covalent Organic Cages Attached to Metal Organic Cage. *Chemistry* **2022**, *4* (3), 865−871.
(59) Rouquerol, J.; Llewellyn, P.; Rouquerol, F. Is the BET equation applicable to microporous adsorbents. *Stud. Surf. Sci. Catal.* **2007**, *160* (07), 49−56.

https://doi.org/10.1021/acs.chemmater.3c02775
Chem. Mater. 2024, 36, 567−574